A percolation model of collisionless runaway in two-dimensional magnetic turbulence

2002 J. Phys. A: Math. Gen. 35 3145

(http://iopscience.iop.org/0305-4470/35/14/301)

INSTITUTE OF PHYSICS PUBLISHING JOURNAL OF PHYSICS A: MATHEMATICAL AND GENERAL

J. Phys. A: Math. Gen. **35** (2002) 3145–3161 PII: S0305-4470(02)33638-2

A percolation model of collisionless runaway in two-dimensional magnetic turbulence

K Arzner

Paul Scherrer-Institut, 5232 Villigen, Switzerland

Received 11 February 2002
Published 29 March 2002
Online at stacks.iop.org/JPhysA/35/3145

Abstract

The mobility of charged particles in a stationary, turbulent magnetic field $\boldsymbol{B}(x, z)$ and electric field $\boldsymbol{E} = (0, 0, \mathcal{E})$ is investigated by means of percolation theory. The escape probability is characterized by the point-to-line connectivity $\tau_z(L) = \mathrm{Prob}(\mathbf{0} \leftrightarrow z = L)$ of non-uniform ($\mathcal{E} \neq 0$) subcritical percolation clusters of an equivalent potential model. A general upper bound on $\tau_z(L)$ is derived and verified by numerical simulations, together with auxiliary results on uniform ($\mathcal{E} = 0$) percolation, including the relations $\xi \propto |h - h_c|^{-4/3}$ and $\tau_z(L) \propto L^{-0.1}\,\mathrm{e}^{-L/\xi}$. For $\langle \boldsymbol{B} \rangle \to 0$, runaway occurs similarly to the classical Dreicer scenario, with the Coulomb collisions replaced by deflections on magnetic irregularities. The collisionless analogue of the Dreicer field is $\mathcal{E}_c = 0.24 \frac{q}{m} l \langle B_x^2 + B_z^2 \rangle$, with l the correlation length of the magnetic irregularities.

PACS numbers: 45.50.Dd, 64.60.Ak, 52.65.Pp, 05.50.+q

1. Introduction

If a collisional plasma is exposed to a dc electric field, free acceleration is limited to those particles for which the electric field exceeds the collisional drag (Dreicer 1960). Depending on whether all or only the fastest particles fulfil this 'Dreicer' criterion, bulk acceleration or Ohmic heating is the dominant effect.

The Dreicer criterion does not apply to collisionless populations, which are frequently encountered in astrophysical applications. However, such particles still interact with the ambient magnetic field, and scattering on magnetic turbulence can play the role of Coulomb collisions. The cross section of Coulomb collisions decreases with velocity, and so does the deflection by localized magnetic inhomogeneities. Depending on the ratio of the Larmor radius to the inhomogeneity scale l, different regimes can occur. If the inhomogeneities are weak ($\langle \boldsymbol{B}^2 \rangle \simeq \langle \boldsymbol{B} \rangle^2$) and smooth in the sense that the 'mean' Larmor radius $\rho_{\langle B \rangle} \doteq mv/e|\langle \boldsymbol{B} \rangle|$ fulfils $\rho_{\langle B \rangle} \ll l$, then a drift motion occurs. The existence of adiabatic motion integrals admits a beautiful Lagrangian theory (Littlejohn 1981) and a well-developed perturbative

description by quasi-linear diffusion (e.g. Schlickeiser 2002). There is no free acceleration across $\langle \boldsymbol{B} \rangle$. Another situation arises for strong ($\langle \boldsymbol{B}^2 \rangle \gg \langle \boldsymbol{B} \rangle^2$) inhomogeneities if the mean Larmor radius exceeds the system size L_s. If, furthermore, the 'Larmor radius' due to fluctuations $\rho_{\delta B} \doteq vm/e\sqrt{\langle \boldsymbol{B}^2 \rangle - \langle \boldsymbol{B} \rangle^2}$ is comparable to the inhomogeneity scale, the orbits can efficiently perforate across the mean magnetic field. Of particular interest is the situation where the inhomogeneity scale is much smaller than the system size

$$l \sim \rho_{\delta B} \ll L_s \leqslant \rho_{\langle B \rangle} \tag{1}$$

which represents homogeneous, strong magnetic turbulence as found, for example, in numerical simulations of the Earth magnetotail (Arzner and Scholer 2001). If an electric field is applied to charged particles in the magnetic turbulence (1), they may become freely accelerated. Some aspects of this process have been described, in a geophysical context, in terms of non-classical diffusion (Gefen *et al* 1983) by Milovanov and Zelenyi (1995) and Treumann (1997) (among others), and modelled numerically, for example, by Ambrosiano *et al* (1988) and Greco *et al* (2000).

The aim of this paper is to work out a non-perturbative, collisionless analogue to the classical Dreicer scenario for the situation (1). The approach is based on the percolation theory, with emphasis on the validation of analytical predictions by numerical simulations. The particles are regarded as test particles. The set-up of the model is guided by the fact that the transition to free acceleration takes place in a regime where adiabaticity breaks down and exact orbits are essential, which rely on conservation laws and symmetries. On the other hand, the onset of runaway bears the characteristics of a percolation problem, where most exact results are available in two (or $\geqslant 6$) dimensions. It is therefore quite natural to consider a model with one ignorable space coordinate and highly complicated (turbulent) dependence on the others. The results of this restricted, yet exact, model are attempted to provide useful benchmarks for more complicated situations.

The organization of this paper is as follows. Section 2 formulates the particle dynamics and gives the condition for unbounded motion in the absence of an electric field. Sections 3 and 4 contain the generalization to a non-vanishing electric field; this is done in several steps. As a main result, a general upper bound on the point-to-line connectivity of non-uniform percolation is derived, together with a criterion for free acceleration (section 5) similar to the Dreicer condition. The results are summarized and discussed in section 6.

2. Two-dimensional particle dynamics

Consider classical particles in a stationary ($\partial_t = 0$) electromagnetic field with $\partial_y = 0$ and an irregular behaviour in $\boldsymbol{r} \doteq (x, z)$. This configuration represents planar MHD turbulence, i.e. helical magnetic surfaces, which are among the most general known MHD equilibria (Edenstrasser 1980). Neglecting the time-dependence of $\boldsymbol{B}$ restricts the validity of the model to particles which are fast compared to the Alfvén velocity. The gyration about in-plane magnetic field lines corresponds to oscillation in an equivalent potential, and it is easily verified that the in-plane motion can be written as

$$m\ddot{\boldsymbol{r}} = -\frac{\partial \Phi}{\partial \boldsymbol{r}} + q\dot{\boldsymbol{r}} \times B_y(\boldsymbol{r})\hat{\boldsymbol{y}} \tag{2}$$

with the equivalent potential

$$\Phi(\boldsymbol{r}) = \frac{(P_y - qA_y(\boldsymbol{r}))^2}{2m} + q\phi(\boldsymbol{r}). \tag{3}$$

Here $P_y = mv_{y0} + qA_y(\boldsymbol{r}_0)$ is the (conserved) canonical momentum, and $\phi(\boldsymbol{r})$ is the electric potential. By convention, $\langle A_y \rangle = 0$, where angular brackets denote a space or ensemble

average. The canonical momentum has contributions from both fields and particles, and their relative weight has a simple physical interpretation,

$$\frac{qA_y}{mv_y} \simeq \frac{l}{r_L}$$

where $r_L = mv_y/q\sqrt{\langle B_x^2 + B_z^2\rangle}$ is a 'Larmor radius' due to the out-of-plane velocity. Thus, dominant field (mechanic) contributions correspond to adiabatic (non-adiabatic) orbits. Clearly, the motion (2) is restricted to

$$\Phi(\boldsymbol{r}) \leqslant E \tag{4}$$

with $E = \frac{m}{2}|\boldsymbol{v}_0|^2 + q\phi(\boldsymbol{r}_0)$. Equation (4) is similar, but not equivalent, to the field line tying theorem of Jones *et al* (1998). In the following, $A_y(\boldsymbol{r})$ is modelled by a centred Gaussian random field (Adler 1981) with variance σ^2 and Gaussian two-point function of correlation length l; the magnetic field thus is a Gaussian random field with $\langle B_x\rangle = \langle B_z\rangle = 0$, and it is assumed that $m^2\langle v_x^2 + v_z^2\rangle/q^2\langle B_y^2\rangle > l^2$, so that gyration about B_y does not hinder particles to explore their energetically accessible domain (4). Note that equation (2) does not involve any approximation, and is able to model the transition from adiabatic to chaotic orbits.

Particles can become unbounded if the domain (4) is globally connected. Using the methods of percolation theory (Isichenko 1992, Nakayama *et al* 1994, Grimmet 1999, Milovanov and Zimbardo 2000) it can be shown that in the absence of an electric field there exists a critical energy E_c^0, below which particles are bounded with probability one (Arzner *et al* 2002):

$$E_c^0 = \frac{P_y^2}{2m} \qquad \text{for} \quad \phi = 0. \tag{5}$$

Equation (5) follows from the critical level $h_c = 0$ of the potential model $A_y(\boldsymbol{r}) \leqslant h$. Particles with $E > E_c^0$ have a strictly positive probability to be in the (unique) infinite cluster. Once within this cluster, the motion is likely to be 'ergodic' so that particles eventually spread out over the whole accessible domain. For subcritical particles $\left(E < E_c^0\right)$ the condition $m^2\langle v_x^2 + v_z^2\rangle/q^2\langle B_y^2\rangle > l^2$ is satisfied, on average, if $2\langle B_y^2\rangle < \langle B_x^2 + B_z^2\rangle$; in what follows it is supposed that $\langle B_y\rangle < mv/qL_s$ ($\to 0$ for $L_s \to \infty$), which is more restricting.

Now let an electric field $\boldsymbol{E} = \mathcal{E}\hat{\boldsymbol{z}}$ be present, which is weak in the sense that the electric potential drop $q\mathcal{E}l$ is much smaller than the fluctuations of Φ (the precise condition is given in equation (19)). The electric field gives rise to a tilted potential, and originally trapped particles run away as soon as the accessible potential saddles have sufficiently declined. In order to work out this process, we adapt a 'graded percolation' argument (Trugman and Weinrib 1983, Sapoval *et al* 1985, Ziff and Sapoval 1986, Roux *et al* 1990). Qualitatively, the argument is as follows. *In the absence of an electric field, a particle with subcritical energy $E < E_c^0$ visits a connected cluster of typical (finite) size, say, L. In the presence of an electric field, the motion along z leads to an energy gain $E = q\mathcal{E}L$. The particle is expected to escape if the energy gain exceeds the potential fluctuations.* A rough estimate is to set $L = \xi_0$, with ξ_0 the correlation length of the connected domains for $\mathcal{E} = 0$. The escape criterion, valid for weak electric fields, then becomes $E + q\mathcal{E}\xi_0 \geqslant E_c^0$. The present paper proposes a similar, yet more refined description in terms of the escape probability of a particle which is initially located at $z = 0$.

3. Connectivity

The escape probability depends on the connectivity of percolating domains, to which this section is devoted. Well-known lattice results are adapted and generalized to the continuum

model (4), with intermediate steps verified by simulations; numerical coefficients which are not predicted by theory are determined from simulations.

3.1. Lattice results

Most theoretical results have been established for lattice percolation, and we begin with a brief outline of the lattice case. The percolation process itself comes in two variants: site and bond percolation. In site percolation, a cluster consists of pairwise adjacent 'occupied' vertices, whereas in bond percolation it is the nearest-neighbour bond which is 'open' or 'closed'. In any case, the sites or bonds are independent of each other, and 'occupied' or 'open' with probability p, and 'vacant' or 'closed' with probability $1 - p$. For uniform percolation (p independent of position) there exists a critical probability p_c, above which an infinite connected cluster occurs with probability one. Sections 3.1–3.4 will be concerned with this uniform case only.

There appear several characteristics of connected clusters in the literature. For our purpose, the relevant characteristic is the connectivity. Following Grimmet (1999) for (bond) percolation on the square lattice, the connectivity $\tau(\mathbf{0}, e_n)$ is defined as the probability that the origin $\mathbf{0} = (0, 0)$, if belonging to a cluster, is connected to the point $e_n = (0, n)$. In the subcritical phase ($p < p_c$), where clusters are finite, the connectivity $\tau(\mathbf{0}, e_n)$ decays exponentially with distance, $\tau(\mathbf{0}, e_n) \sim \mathrm{e}^{-n/\xi}$, where the sign '$\sim$' indicates that

$$\lim_{n\to\infty} -\frac{1}{n} \ln \tau(\mathbf{0}, e_n) = \frac{1}{\xi} < \infty. \tag{6}$$

Throughout this paper, the correlation length ξ is defined by equation (6) (and not by the rms cluster radius as used, for example, by Hoshen 1997). Note that the limit (6) is relatively weak, and allows for power law corrections to the exponential decay.

For the present application, the foregoing definition of connectivity is adapted as follows. We consider the infinite square lattice, and define the point-to-line connectivity $\tau_z(n)$ as the probability that the origin is connected to the line $z = n > 0$, if it is in a connected cluster. (This conditioning is automatically satisfied by a particle in the potential (3).) Normalization is such that $\tau_z(0) = 1$. The probability $\tau_z(n)$ is well defined and does not collapse to a zero–one law when the system size goes to infinity. Note that the path connecting the origin to the line $z = n$ is allowed to pass at $z < 0$, and that the following inequality holds:

$$\tau(\mathbf{0}, e_n) \leqslant \tau_z(n) \leqslant \sum_{x=-\infty}^{\infty} \tau(\mathbf{0}, (x, n)). \tag{7}$$

See Grimmet (1999) for a formal proof of similar results involving the FKG inequality (Harris 1960, Fortuin *et al* 1971). From numerical simulations, the connectivity $\tau_z(n)$ is found to follow closely an exponential law down to $n \gtrsim 0.3\xi$ (figure 1)—an advantage which is not shared by other characteristics such as the spanning probability $\pi_z(n, w)$ across a box of width w and height n, or the cluster radius distribution $\rho_z(n)$, which are shown for comparison in figure 2. In fact, the almost-exponential decay of $\tau_z(n)$ is in agreement with the analytic results of Campanino *et al* (1991), who showed for bond percolation on the d-dimensional hypercubic lattice that $\tau(\mathbf{0}, (0, 0, \ldots, n)) \to A(p)n^{(1-d)/2}\,\mathrm{e}^{-n/\xi}$, and that $\sum_{x\in\mathbb{Z}^{d-1}} \tau(\mathbf{0}, (x, n))$ decays purely exponentially with n (the leading power law correction is n^0). With regard to equation (7), we thus make the ansatz

$$\tau_z(n) \to a_0 n^{\chi}\,\mathrm{e}^{-n/\xi} \tag{8}$$

with the same correlation length ξ as in $\tau(\mathbf{0}, e_n)$ (see appendix B) and some χ satisfying $-1/2 \leqslant \chi \leqslant 0$. The asymptotic form ($\to$) indicates that the ratio of the left-hand and

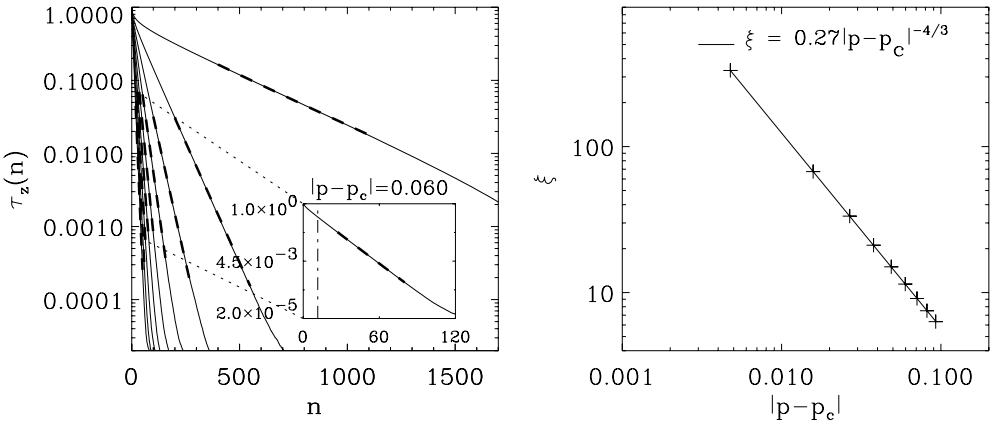

Figure 1. Point-to-line connectivity (left, solid line) from numerical simulations of site percolation on a square 2048^2 lattice, and its analytical representation by equation (8) (dashed). Different curves represent different values of $|p - p_c|$ with $p_c = 0.592\,76$; the case $|p - p_c| = 0.06$ is shown in exploded view. Right: simulated (crosses) and theoretical (solid line) correlation length.

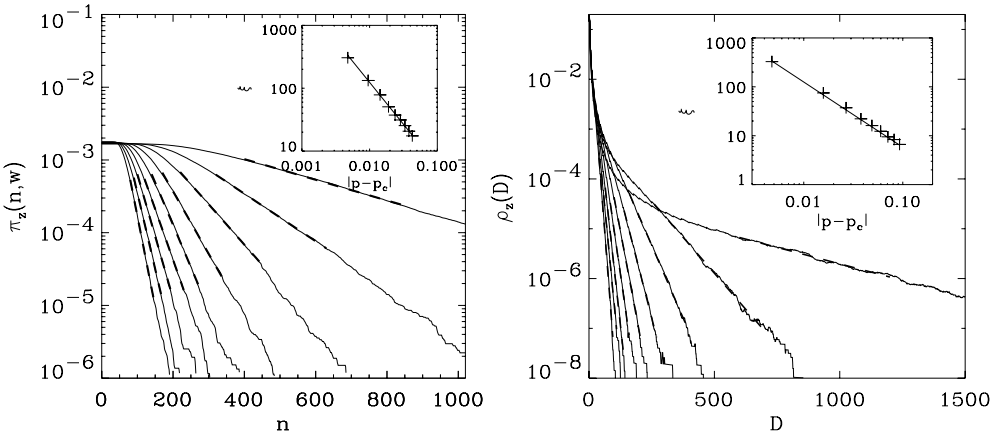

Figure 2. Left: the spanning probability $\pi_z(n, w)$ across a box of width $w = 1024$ and height n (cyclic boundaries in x). Right: cluster diameter distribution $\rho_z(D)$, with $D = \max|z_i - z_j|$. Insets: empirical correlation lengths (crosses) according to equation (6); the solid lines represent equation (9), with $\kappa_0 = 0.27$ and $p_c = 0.592\,76$. Note that $\pi_z(n, w)$ and $\rho_z(D)$ have the same asymptotic behaviour in the sense of equation (6), but appreciably deviate from it at $n, D < \xi$.

right-hand sides of equation (8) converges to unity as $n \to \infty$. The normalization coefficient a_0 depends on $\tau_z(n)$ at $n \ll \xi$, and must be determined numerically.

3.2. Correlation length

The correlation length ξ is a function of p and diverges as $p \uparrow p_c$. The divergence is believed to be of the form

$$\xi = \kappa_0 |p - p_c|^{-\nu} \tag{9}$$

with κ_0 a numerical factor of order unity (which cannot be derived from scaling arguments), and the presumably exact result $\nu = 4/3$ (Nienhuis *et al* 1980, Riedel 1981), which is supported

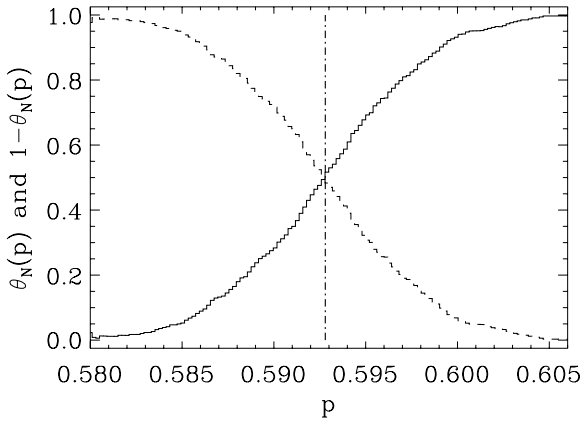

Figure 3. The spanning probability $\theta_N(p) = n_c/(n_c + n_d)$ (solid line) and its complement $1 - \theta_N(p)$ (dashed) across a square lattice of linear size $N = 1024$. n_c (n_d) is the number of connected (disconnected) realizations in an ensemble of 50 000 realizations. The empirical critical probability, defined by $\theta_N(p) = 1/2$, is $p_c = 0.592\,76 \pm 0.000\,04$.

by numerical simulations (e.g. Hoshen 1997, $\nu = 1.320 \pm 0.002$). The critical probability p_c depends on the lattice type and percolation model; for bond percolation on the square lattice $p_c = 1/2$ (Sykes and Essam 1964, Kesten 1980), and for site percolation on the square lattice $p_c = 0.592\,7460 \pm 0.000\,000\,05$ (Ziff 1992). The latter value is known numerically only and is subject to finite size effects. Site percolation on a square lattice represents the digital zero-correlation limit of the continuous field used in the present simulations (see appendix A).

Figure 1 shows, as a benchmark test of the present code, the numerical verification of equation (8) for site percolation on a square lattice of size 2048^2. The connectivity is evaluated from 20 000 realizations with double periodic boundary conditions. Different graphs represent different values of $|p - p_c|$; for better clarity, the case $|p - p_c| = 0.06$ is shown as an exploded view (inset). The critical probability $p_c = 0.592\,76 \pm 0.000\,04$ is taken from an independent simulation of the spanning probability of a lattice of half size ($N = 1024$) with non-periodic boundaries (figure 3), where p_c is defined by the cross-over of the top–bottom connection (disconnection) probabilities, which provides a robust estimate (Ziff 1992) of the finite-size critical probability of the present simulation. The sample size underlying figure 3 is 50 000.

Equation (8) was fitted to each curve of figure 1 (left), and the resulting correlation lengths ξ are shown in figure 1 (right, crosses), together with the theoretical prediction (9) for $\kappa_0 = 0.267$ and $\nu = 4/3$ (solid line). The estimates are derived from the dashed segments (figure 1, left) which represent equation (8) with $a_0 = 1.02$ (independently of p) and $\chi = -0.1$. Assuming Poisson errors, the reduced chi square is $\chi^2_{\min} = 1.4$. If the parameters (a_0, χ, κ_0, ν) are jointly estimated from the full set of Monte Carlo data, one finds that $a_0 = 1.05 \pm 0.06$, $\chi = -0.11 \pm 0.015$, $\kappa_0 = 0.267 \pm 0.007$ and $\nu = 1.3325 \pm 0.003$. The errors are not independent of each other, and represent worst-case estimates based on a $4\chi^2_{\min}$-deviation (see figure 4). In addition to the statistical errors there are systematic errors which depend on the selection of fitting intervals. By varying the latter, it was found that the systematic errors are of the same order as the statistical errors, and dominate for sample sizes $\gtrsim 10^4$. To summarize, the different methods for determining the parameters (a_0, χ, κ_0, ν) agree within the errors of the simulation, and are compatible with the theoretical results $\nu = 4/3$ and $-1/2 \leqslant \chi \leqslant 0$.

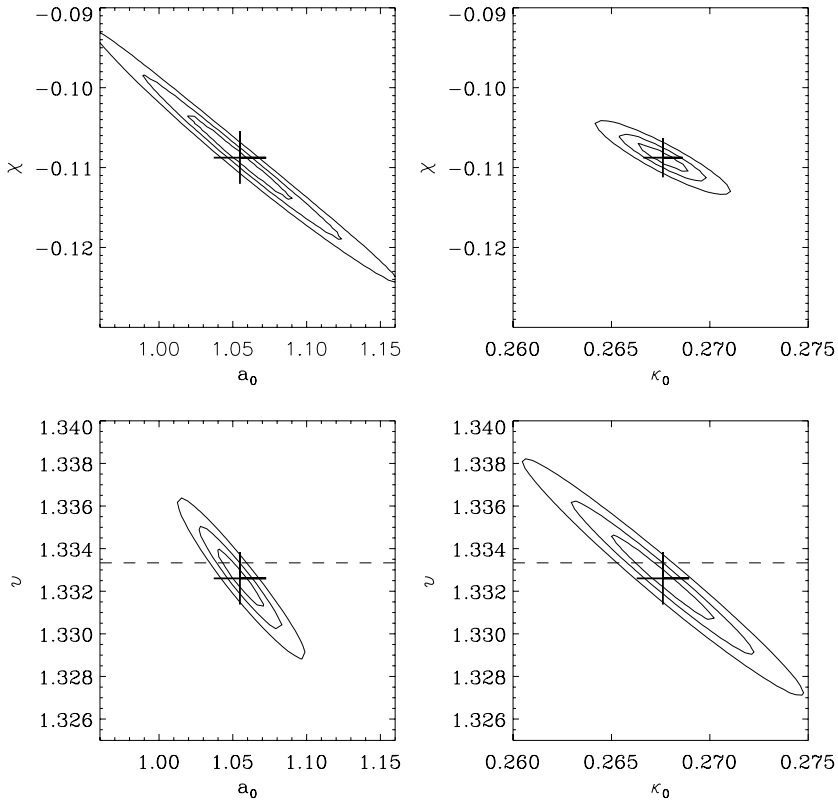

Figure 4. Joint estimate of the parameters a_0, χ, κ_0, ν from the Monte Carlo data (figure 1). The contours represent chi-square levels $\chi^2 = (2, 4, 8) \cdot \chi^2_{\min}$ assuming purely statistical (Poisson) errors. The theoretical value $\nu = 4/3$ is indicated by a dashed line.

3.3. Sign-symmetric, continuous field

Equations (8)–(9) were established for a discrete lattice rather than for a continuous field such as $A_y(\boldsymbol{r})$. Following a suggestion by Weinrib (1982), the lattice results (8)–(9) can be translated to the excursion set $G(\boldsymbol{r}) \leqslant h$ of a continuous sign-symmetric random field $G(\boldsymbol{r})$ by associating the maxima of $G(\boldsymbol{r})$ with the 'lattice' vertices, and the saddle points of $G(\boldsymbol{r})$ with the 'lattice' bonds. The term 'lattice' is put into quotation marks since the 'lattice' has, in general, an irregular structure. The probability p of the discrete case is related to the normalized saddle point density $p_s(h)$ according to $p = \int_{-\infty}^{h} p_s(h)\,\mathrm{d}h$, and p_c corresponds to the critical level $h_c = 0$ (in two dimensions). For Gaussian random fields (Adler 1981) the normalized $\left(\int_{-\infty}^{\infty} p_s\,\mathrm{d}h = 1\right)$ saddle point density has a point set representation and can be obtained from a straightforward calculation. In the case of a Gaussian two-point function $\langle G(0)G(\boldsymbol{r})\rangle = \sigma^2\,\mathrm{e}^{-r^2/2l^2}$, the result is

$$p_s(h) = (3/4\pi)^{1/2}\sigma^{-1}\,\mathrm{e}^{-3h^2/4\sigma^2}.$$

Expanding $p_s(h)$ about $h = h_c$, one finds that $|p - p_c| \simeq (3/4\pi)^{1/2}\sigma^{-1}|h - h_c|$ and

$$\xi = (4\pi/3)^{\nu/2}\kappa l|(h - h_c)/\sigma|^{-\nu} \tag{10}$$

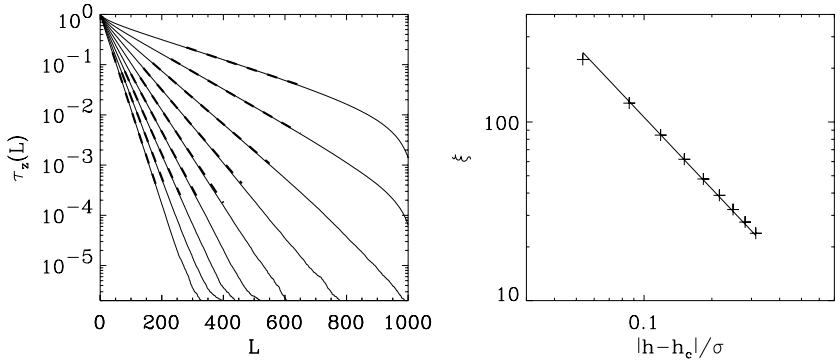

Figure 5. Similar to figure 1, but for a 'continuous' Gaussian random field G with correlation length $l = 2$ and variance $\sigma^2 = 1$, cut at threshold h. The critical energy of this configuration is $h_c = 0.014$; the linear system size is 1024^2.

for some numerical factor κ. In the derivation of equation (10) it was used that $e^{-3h_c^2/4\sigma^2} = 1 + o(h_c^2)$, with $h_c = 0$ for theoretical, and $h_c \approx 0$ for numerical realizations. The continuous version of equation (8) is

$$\tau_z(L) \to a \left(\frac{L}{l}\right)^{\chi} e^{-L/\xi}. \tag{11}$$

According to the universality hypothesis (e.g. Fisher 1983), the critical behaviour is independent of the details of the lattice structure in a given dimension; hence, ν and χ should be the same as in the discrete case. This conjecture is supported by numerical simulations. Figure 5 shows the results from a numerical experiment similar to figure 1, but with the Poisson lattice replaced by a 'continuous' (see appendix A) centred Gaussian random field G with variance $\sigma^2 = 1$ and correlation length $l = 2.5$ lattice constants. The linear system size is $N = 1024$, and double periodic boundary conditions are applied. The accessible regions are $G(\boldsymbol{r}) \leqslant h$. The empirical critical threshold of this random field, obtained from spanning probabilities, is $\langle h_c \rangle = 0.014$. Figure 5 (left) shows the connectivity $\tau_z(L)$ for different values of $|h - h_c|/\sigma$ of a sample of 30 000 realizations of $G(\boldsymbol{r})$. Again, $\tau_z(L)$ decays asymptotically exponentially if $L \gtrsim 0.3\xi$, and the empirical dependence of ξ on $|h - h_c|/\sigma$ is compatible with equation (10) (figure 5 right). Similar simulations as in figure 5 were repeated with various l ranging from 1 to 16 lattice constants. From these runs, the validity of equations (10)–(11) is confirmed and the numerical coefficients are found to be $a = 1.15 \pm 0.08$, $\kappa = 0.8 \pm 0.05$ and $\chi = -0.1 \pm 0.03$. For fixed N/l, the critical threshold h_c decreases with increasing l towards the theoretical limit $h_c = 0$.

3.4. Interlude: finite-size effects

It can be noted from figure 5 that the Monte Carlo results drop somewhat below the analytical prediction as $h \to h_c$, which is a consequence of the finite system size (cf Ziff 1992). The connectivity becomes affected by the finite system size (N) whenever ξ becomes comparable to N. Since the lattice simulations allow larger N/ξ than the continuum simulations, the finite-size effects are studied from lattice runs. Increasing N for a fixed value of p, and determining ξ as in figure 1, it is found that ξ is generally under-estimated if $\xi \ll N$. Figure 6 shows an example of lattice (site) percolation for the case $p = 0.583\,25$ ($< p_c$). The system size is increased in powers of 2 from $N = 64$ to $N = 2048$. The theoretical value $\xi = 0.267|p - p_c|^{-\nu}$ is

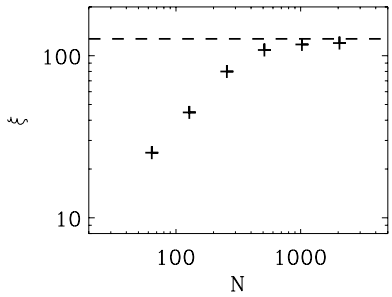

Figure 6. The dependence of the correlation length ξ on the system size N for fixed $|p - p_c| = 0.0095$.

indicated by a dashed line (averaged over 3000 samples). As can be seen from figure 6, $\xi(N)$ monotonically approaches the theoretical value. This behaviour was found to be generic: quite naturally, ξ becomes under-estimated in a finite system approaching criticality. Within the limited range of scales of the present 'brute force' (full lattice) simulation, deviations of the relation $\nu = 4/3$ can be attributed to the finite system size N, and the relation $\nu = 4/3$ is consistent with the extrapolation $N \to \infty$.

3.5. Equivalent potential

Equation (10) holds for a sign-symmetric random field. In order to apply it to the potential (3), the accessible domain (equation 4)) is first rewritten in the dimensionless form

$$(\eta - G)^2 - \epsilon z^* \leqslant E^* \tag{12}$$

with $A_y = \sigma G, \langle G^2 \rangle = 1, z^* = z/l, \eta = P_y(q\sigma)^{-1}, E^* = 2mE(q^2\sigma^2)^{-1}, \epsilon = 2m\mathcal{E}l(q\sigma^2)^{-1}$. Thus, lengths are normalized by the magnetic inhomogeneity scale, the canonical momentum is normalized by the field momentum (and similar for the energy), and the electric field is characterized by the relative voltage drop across a magnetic inhomogeneity. Besides a simplification of notation, equation (12) reveals the physical parameters on which the escape energy solely depends: E^* is a function of the dimensionless canonical momentum (η) and the dimensionless electric field (ϵ).

Let us proceed with the 'graded percolation' of the beginning of section 3, and start with the uniform case $\epsilon = 0$. In dimensionless form, the accessible domain is $\mathcal{G} \doteq \{(G-\eta)^2 \leqslant E^*\}$ with $E^* \leqslant \eta^2$ (subcritical phase), and we are interested in the probability that the origin, if belonging to $\mathcal{G}$, is connected to the line $z = L$. The complement of $\mathcal{G}$ contains an infinite connected domain $\bar{\mathcal{G}}^\infty$, and $\mathcal{G}$ has two types of borders: interior (with holes) and exterior (with $\bar{\mathcal{G}}^\infty$) (figure 7). Obviously, it is the latter which is relevant for the asymptotic behaviour of the connectivity. When expressed in terms of G, to which equations (10)–(11) apply, the accessible domain becomes $\{\eta - \sqrt{E^*} \leqslant G \leqslant \eta + \sqrt{E^*}\}$. Its complement is $\bar{\mathcal{G}} = \bar{\mathcal{G}}_1 \cup \bar{\mathcal{G}}_2$, with $\bar{\mathcal{G}}_1 = \{G < \eta - \sqrt{E^*}\}$ and $\bar{\mathcal{G}}_2 = \{G > \eta + \sqrt{E^*}\}$. Depending on the sign of η, $\bar{G}^\infty$ is either within $\bar{\mathcal{G}}_1$ (if $\eta > 0$) or within $\bar{\mathcal{G}}_2$ (if $\eta < 0$). (This is so because of sign $(\eta \pm \sqrt{E^*}) = \mathrm{sign}(\eta)$, and because the critical threshold of G is zero.) If $\bar{G}^\infty$ is within $\bar{\mathcal{G}}_1$, then the maximal accessible domain (limited by exterior borders) is $\mathcal{G}_1 = \{G \geqslant \eta - \sqrt{E^*}\}$; if $\bar{G}^\infty$ is within $\bar{\mathcal{G}}_2$, then the maximal accessible domain is $\mathcal{G}_2 = \{G \leqslant \eta + \sqrt{E^*}\}$. Both cases are combined in

$$\mathcal{G}' \doteq \{\mathrm{sign}(\eta)G \geqslant |\eta| - \sqrt{E^*}\}. \tag{13}$$

By construction, $\mathcal{G} \subseteq \mathcal{G}'$, and the domain $\mathcal{G}'$ differs from $\mathcal{G}$ only by the absence of interior holes (figure 7), so that $\mathcal{G}$ and $\mathcal{G}'$ have the same correlation length in the sense of equation (6).

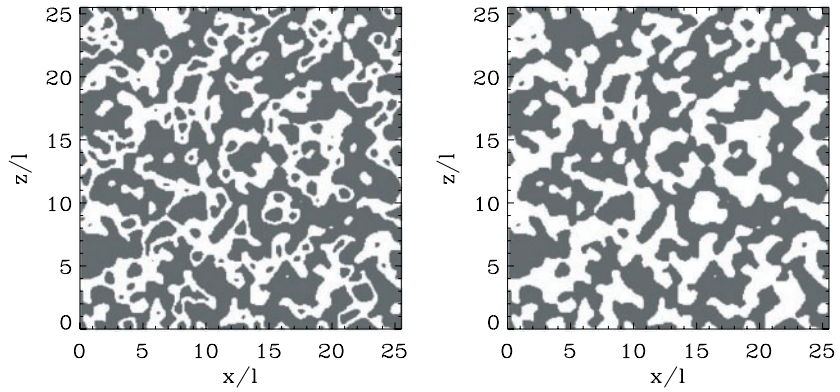

Figure 7. Accessible (white) and forbidden (grey) regions of the domains $\mathcal{G} \doteq (G-\eta)^2 \leqslant E^*$ (left) and $\mathcal{G}' \doteq \mathrm{sign}(\eta)G \geqslant |\eta| - \sqrt{E^*}$ (right); both are in the subcritical phase with $\eta = -0.8$, $E^* = 0.5$.

As G is sign-symmetric, the factor 'sign(η)' in equation (13) does not matter when considering a statistical average. Equation (10) therefore predicts that

$$\xi = (4\pi/3)^{\nu/2}\kappa l||\eta| - \sqrt{E^*} + h_c|^{-\nu} \qquad \text{for} \quad \epsilon = 0 \tag{14}$$

where h_c has been retained to account for numerical realizations. Now let $\epsilon > 0$, and consider the behaviour of the domains $\mathcal{G} = \{(G-\eta)^2 \leqslant E^* + \epsilon z^*\}$ and $\mathcal{G}' = \{\mathrm{sign}(\eta)G \geqslant |\eta| - \sqrt{E^* + \epsilon z^*}\}$. Note that $\epsilon > 0$ implies $z > -E^*/\epsilon$, the physical reason for which is energy conservation in the magnetic irregularities, so that the electric potential imposes a strict limit on the accessible domain. For $\epsilon > 0$, both $\mathcal{G}$ and $\mathcal{G}'$ contain unique connected domains $\mathcal{G}^\infty$ and $\mathcal{G}'^\infty$, which extend to $z = +\infty$. The relation $\mathcal{G} \subseteq \mathcal{G}'$ holds pointwise and therefore also for $\epsilon > 0$. As a consequence, one has that $\mathcal{G}^\infty \subseteq \mathcal{G}'^\infty$ because $\mathcal{G}$ and $\mathcal{G}'$ coincide at $z \to \infty$. It follows that $\mathcal{G}'$ and $\mathcal{G}$ have the same correlation length also, if there is an electric field.

The quantity of interest is the probability that a particle which is initially at $z = 0$ can visit $z = L$; such a particle is *a priori* in its energetically accessible domain $\mathcal{G}$, and therefore also in $\mathcal{G}'$. Its geometrical probability to visit $z = L$ is thus characterized by the (common) correlation length of $\mathcal{G}$ and $\mathcal{G}'$.

4. Escape probability

In the presence of an electric field, the particles gain energy when moving along z, which amounts to a continuous increase in the correlation length $\xi(z)$. In terms of lattice percolation, $\epsilon > 0$ corresponds to non-uniform percolation with $\partial p/\partial n > 0$.

It is not trivial to calculate the exact connectivity of non-uniform percolation, but it is rather easy to obtain a good upper bound. For the sake of simplicity this is derived for lattice percolation, and its continuum version is verified by numerical simulations. The strategy is to decompose $\tau_z(n)$ into a chain of conditional probabilities $\tau_z(k|k-1)$, and to establish inequalities between the non-uniform conditional probabilities and their uniform counterparts. We start with some necessary definitions and prerequisites.

All points of the line $z = n \geqslant 0$, which are connected to the origin, are either accessible through $z \leqslant n$ ('direct' connections), or through excursions to $z > n$ ('indirect' connections). See figure 8 for a clarification. It is the 'direct' connections which are relevant for the event $\{\mathbf{0} \leftrightarrow z = n\}$, since each 'indirect' connection relies on a 'direct' one. Let $\tau_z(n|n-1)$

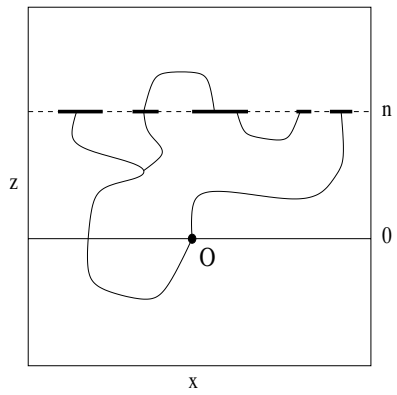

Figure 8. Direct and indirect connections of the origin (O) to the line $z = n$. There are three directly, and two indirectly connected intervals.

be the probability that the origin is connected to the line $z = n$, conditional to being connected to the line $z = n - 1$. Note that $\tau_z(n|n-1) = \tau_z(n)/\tau_z(n-1)$ because $\mathrm{Prob}(\{\mathbf{0} \leftrightarrow z = n\} \cap \{\mathbf{0} \leftrightarrow z = n-1\}) = \mathrm{Prob}(\{\mathbf{0} \leftrightarrow z = n\})$. In the uniform case ($p = \mathrm{const}$), $\tau_z(n)$ is given by equation (8) and the conditional probabilities satisfy

$$\tau_z(n+1|n) \to \left(\frac{n+1}{n}\right)^{\chi} \mathrm{e}^{-1/\xi(p)} \leqslant \mathrm{e}^{-1/\xi(p)}. \tag{15}$$

The event $\{\mathbf{0} \leftrightarrow z = n-1\}$ implies that there is at least one point, say $(x, n-1)$, which is connected to the origin. In general, there are further such points on the line $z = n-1$, and we are interested in those m of them which are connected to $(x, n-1)$ by 'direct' paths, and are relevant to the extinction event $\{\mathbf{0} \leftrightarrow z = n-1\} \cap \{\mathbf{0} \not\leftrightarrow z = n\}$. By the independence of the individual sites (or bonds), the extinction probability is $(1-p)^{m+1}$, and therefore $\tau_z(n|n-1) = 1 - (1-p)^{m+1}$. Note that the extinction probability is the same for both site and bond percolation on the square lattice, and that it is a decreasing function of m. Consider now the non-uniform case with $\partial p/\partial n \geqslant 0$ at some fixed $n = n_0$. Compared to the uniform case with uniform probability $p(n_0)$, a positive gradient favours 'indirect' connections and suppresses 'direct' ones, so that m is expected to become smaller and, therefore (without complete rigour),

$$\tau_z^i(n_0|n_0-1) \leqslant \tau_z^0(n_0|n_0-1) \qquad \forall n_0 : 0 \leqslant p(n_0) < p_c \tag{16}$$

where $\tau_z^i(n_0|n_0-1) = \tau_z(n_0|n_0-1;\, p = p(n))$ and $\tau^0(n_0|n_0-1) = \tau_z^0(n_0|n_0-1;\, p = p(n_0))$. The non-uniform connectivity can be written as $\tau_z(n) = \tau_z^i(n|n-1)\tau_z^i(n-1|n-2)\ldots\tau_z^i(1|0)\tau_z(0)$. Each factor in this chain satisfies equations (16) and (15), so that

$$\begin{aligned}
\tau_z(n) &= \tau_z^i(n|n-1)\tau_z^i(n-1|n-2)\ldots\tau_z^i(1|0) \\
&\leqslant \tau_z^0(n|n-1)\tau_z^0(n-1|n-2)\ldots\tau_z^0(1|0) \\
&\simeq \prod_k \left(\frac{k}{k-1}\right)^{\chi} \mathrm{e}^{-1/\xi(p(k))} \\
&\simeq a_0 n^{\chi} \exp\left[-\sum_{k=1}^{n} 1/\xi(p(k))\right].
\end{aligned} \tag{17}$$

The normalization factor a_0 has been introduced to obtain agreement with the uniform case. The continuous version of inequality (17) is

$$\tau_z(L) \lesssim a \left(\frac{\tilde{L}}{l}\right)^{\chi} \exp\left(-\int_0^{\tilde{L}} \frac{\mathrm{d}z}{\xi(z)}\right) \tag{18}$$

where $\xi(z) = (4\pi/3)^{\nu/2}\kappa l|\eta| - \sqrt{E^* + \epsilon z/l}|^{-\nu}$, $\tilde{L} = \min(L, z_{\max})$, and $z_{\max} = l(\eta^2 - E^*)/\epsilon$ is a cut-off at which $\xi(z)$ diverges; the dimensionless parameters (η, E^*, ϵ) are as in equation (12). For $\epsilon = 0$, equation (18) reduces to equation (11). Equation (18) is only valid if $z_{\max} \gg 0.3\xi(0)$; it is thus restricted to weak electric fields in the sense that

$$\epsilon \ll (\eta^2 - E^*)(|\eta| + \sqrt{E^*})^{\nu}. \tag{19}$$

Equation (19) is not a severe constraint since it is always fulfilled at the onset of runaway. Beyond $z_{\max}$ the connectivity (18) remains constant, and particles are expected to become free. The integral occurring in equation (18) can be calculated explicitly, and one obtains

$$\tau_z(L) \lesssim a \left(\frac{\tilde{L}}{l}\right)^{\chi} \exp\left\{-\left(\frac{3}{4\pi}\right)^{\nu/2} \frac{1}{\epsilon\kappa} f(x, |\eta| + h_c, E^*, \nu)\Big|_{x=0}^{x=\epsilon\tilde{L}/l}\right\} \tag{20}$$

where

$$f(x, a, b, \nu) = 2\frac{a^{2+\nu} + (a - \sqrt{b+x})^{\nu}[(b+x)(1+\nu) - a\nu\sqrt{b+x} - a^2]}{(2+\nu)(1+\nu)}.$$

If $\epsilon = 0$, the right-hand side of equation (18) decays exponentially, but for $\epsilon > 0$ the right-hand side of equation (20) converges to the finite limit $\tau_z(z_{\max})$ which represents the geometrical escape probability ($h_c = 0$ for simplicity):

$$p_e \lesssim a \left(\frac{\eta^2 - E^*}{\epsilon}\right)^{\chi} \exp\left\{-2\left(\frac{3}{4\pi}\right)^{\nu/2} \frac{(|\eta| - \sqrt{E^*})^{1+\nu}(|\eta| + (1+\nu)\sqrt{E^*})}{\epsilon\kappa(2+\nu)(1+\nu)}\right\}. \tag{21}$$

Clearly, the electric field helps particles to escape, indicating $\partial p_e/\partial\epsilon > 0$, which is easily verified for equation (21) with $\chi < 0$. For given values of p_e, ϵ and η, equation (21) has a unique solution for E^* satisfying $\partial E^*/\partial\epsilon \leqslant 0$. As a function of E^*, the right-hand side of equation (21) represents an unsharp step function of width

$$\Delta E^* \simeq \eta^2 - \tfrac{1}{9}(4.8(\epsilon\kappa/|\eta|)^{3/7} - 3|\eta|)^2 \tag{22}$$

centred at $E^* \simeq \eta^2 - \Delta E^*/2$. Equation (20) is a theoretical upper bound derived from an analogue lattice case, and its quality is to be assessed from numerical simulations. Figure 9 shows a comparison, where a solid line represents the simulation and a dashed line represents equation (20). The simulation comprises 80 000 realizations of a $N = 1024$ system with $l = 2.8$, $h_c = 0.012$, and different sets (E^*, η, ϵ). Each realization covers the range $-z_0 \leqslant z \leqslant N - z_0$, where the choice $z_0 = \max(E^*/\epsilon, N/4)$ prevents boundary effects. Connectivity is computed from the distances of random points at $z = 0$ to the top of the connected clusters. The numerical parameters used in equation (20) are in accordance with the homogeneous simulations ($\kappa = 0.79, a = 1.15, \chi = -0.1, \nu = 4/3$). As can be seen from figure 9, equation (20) is rather tight over many decades; numerically, it was found that $0.38 \times \tau_z^{\text{Eq.20}}(L) \leqslant \tau_z^{\text{simulated}}(L) \leqslant 0.57 \times \tau_z^{\text{Eq.20}}(L)$. Similarly, inequality (17) was verified for the lattice case with non-uniform probability $p(n) = p_0 + \epsilon(n - n_0)$. The accuracy of (17) is similar for the continuous case (20).

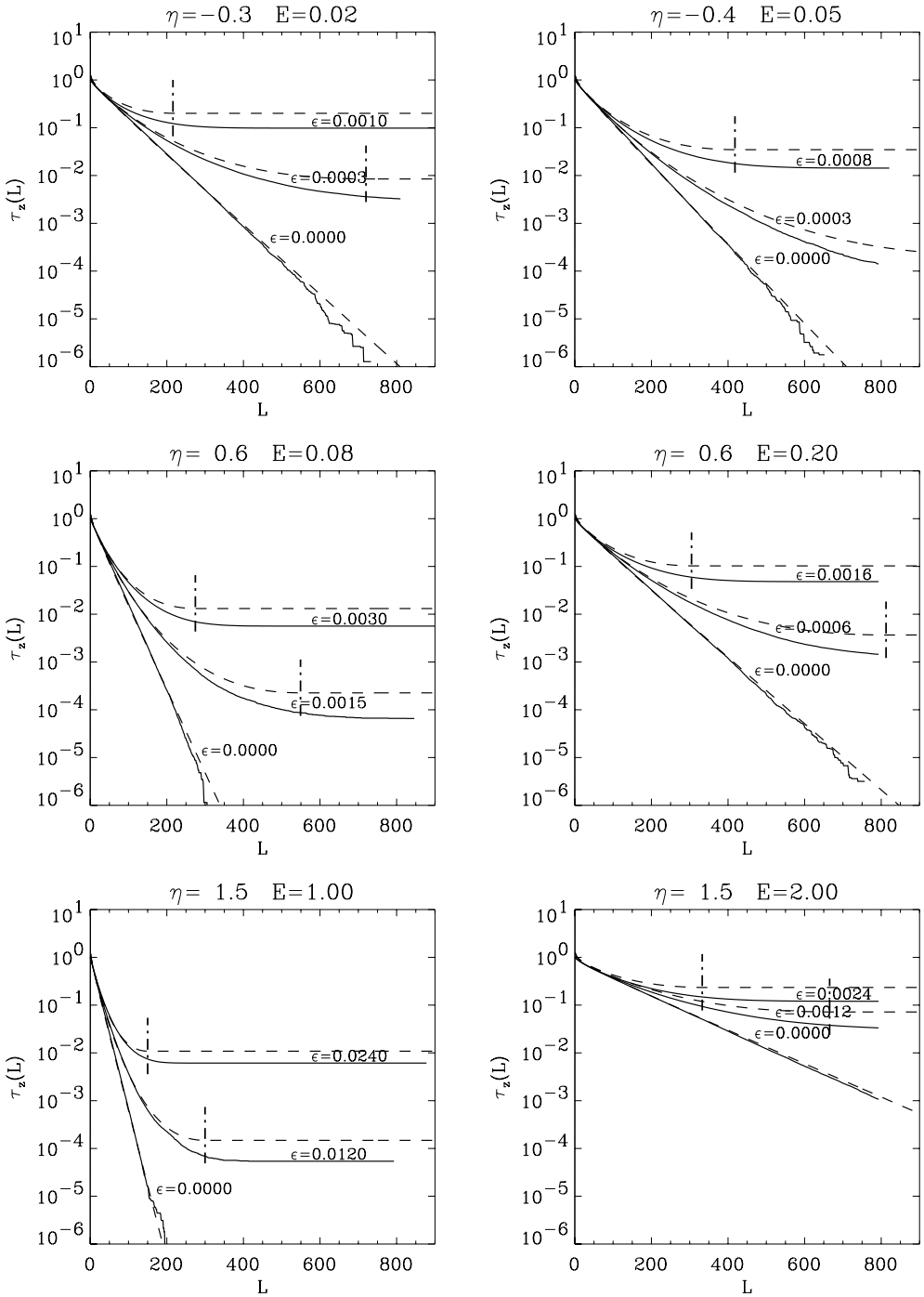

Figure 9. The effect of the electric field (ϵ): simulated connectivity (solid) and upper bound (equation (20), dashed) of the excursion set $\mathcal{G}'$, with $\langle G^2 \rangle = 1$ and $l = 2.8$. Different graphs represent different sets (E^*, η, ϵ); $z_{\max}$ (equation (18)) is marked dotted-dashed. The case $\epsilon = 0$ corresponds to figure 5.

5. 'Collisionless Dreicer field'

We shall now draw a brief analogy with the classical Dreicer field. Within its range of validity (19), equation (21) is dominated by the exponential factor. As a function of ϵ, the escape probability thus behaves like $\mathrm{e}^{-k/\epsilon}$. The graph of this function increases monotonically with ϵ and has a (smooth) shoulder at $\epsilon \simeq 4k$, which can be used to define an escape criterion

$$\epsilon \gtrsim 8\left(\frac{3}{4\pi}\right)^{\nu/2} \frac{(|\eta| - \sqrt{E^*})^{1+\nu}(|\eta| + (1+\nu)\sqrt{E^*})}{\kappa(2+\nu)(1+\nu)}. \tag{23}$$

A particle, which is initially at rest ($E^* = 0$), is thus expected to escape if the electric field exceeds $\epsilon_c = 8(3/4\pi)^{\nu/2}|G(\boldsymbol{r}_0)|^{2+\nu}/\kappa(2+\nu)(1+\nu)$. Averaging over an ensemble of Gaussian fields (or, equivalently, over the particle initial position), one obtains the mean critical field

$$\langle \epsilon_c \rangle = 8\frac{(3/2)^{\nu/2}\Gamma\left(\frac{1}{2}+\frac{\nu}{2}\right)}{\pi^{(1+\nu)/2}(2+\nu)\kappa} = \frac{0.76}{\kappa}.$$

Restoring the physical units, using $\kappa = 0.8$, $\nu = 4/3$, and expressing the variance of the vector potential in terms of the variance of the magnetic field, $\left\langle B_x^2 + B_z^2 \right\rangle = 2\langle A_y^2 \rangle / l^2$, one obtains the acceleration criterion $\mathcal{E} > \mathcal{E}_c$ with

$$\mathcal{E}_c = 0.24\frac{q}{m} l \left\langle B_x^2 + B_z^2 \right\rangle. \tag{24}$$

Within the collisionless model, $\mathcal{E}_c$ plays a similar role to the Dreicer field in a collisional plasma, with scattering on magnetic inhomogeneities replacing the Coulomb collisions. Similar to the Coulomb logarithm, the exact value of the numerical coefficient in equation (24) depends on its actual definition, i.e. on the required escape probability, but is always of the order given by equation (24). Equation (24) has a simple physical interpretation: the voltage drop across an inhomogeneity must exceed some fraction of the equivalent potential fluctuations, which is determined by the percolation theory.

6. Summary and discussion

Starting from the particle dynamics in an irregular magnetic field $\boldsymbol{B}(x, z)$, the problem of free acceleration by an electric field $\boldsymbol{E} = (0, 0, \mathcal{E})$ was reduced to the point-to-line connectivity $\tau_z(L)$ of an equivalent potential model. $\tau_z(L)$ is derived from simulations and from the predictions of percolation theory. The accepted relation $\xi \propto |p - p_c|^{-4/3}$ is confirmed, and the constants of proportionality are determined for both the square lattice and the potential model $G(x, z) \leqslant h$. For uniform percolation it is found that $\tau_z(L) \propto L^{-0.1}\,\mathrm{e}^{-L/\xi}$ in both the lattice and continuous cases, where the power law correction is within the theoretical bounds following from the work of Campanino *et al* (1991). A weak electric field corresponds to non-uniform percolation with slowly varying probabilities; in this case, a general upper bound on $\tau_z(L)$ is derived and confirmed by numerical simulations.

The agreement between the upper bound and the simulation is not too surprising in the light of the following argument: if the derivation equation (18) is repeated for the probability $\bar{\tau}_z(L)$ that a point (x, L) is connected to the line $z = 0$, one obtains $\bar{\tau}_z(L) \gtrsim a(L/l)^{\chi} \exp\left\{\int_L^0 \mathrm{d}z/\xi(z)\right\}$, where the $\gtrsim$ sign arises from the reversed role of direct and indirect connections. Now, as the electric field is weak, there exists a range $\xi(0) \ll L \ll z_{\max}$ for which $\bar{\tau}_z(L) \sim \tau(\mathbf{0}, (0, L)) = \tau((0, L), \mathbf{0}) \sim \tau_z(L)$ (see appendix B). The combination of the upper bound on $\tau_z(L)$ and the lower bound on $\bar{\tau}_z(L)$ then gives that $\tau_z(L) \sim \exp\left\{-\int_0^L \mathrm{d}z/\xi(z)\right\}$, so that the right-hand side of equation (18) gives, at least, the correct logarithmic order.

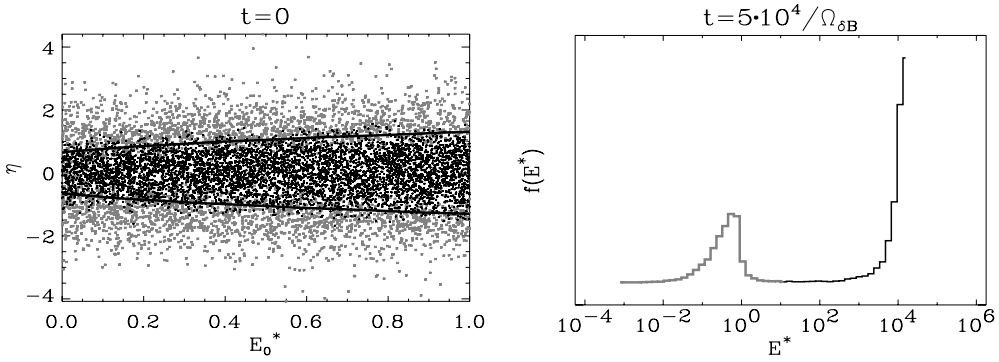

Figure 10. Test particle simulation with Gaussian $A_y(\boldsymbol{r})$ with $l = 20$, system size $N = 512$ (periodic boundaries) and electric field $\epsilon = 0.12$. Left: initial dimensionless kinetic energy (E^*) and canonical momentum (η) of bounded (grey) and free (black) particles; the 'collisionless Dreicer' criterion (23) is marked by a solid line. Right: the energy distribution at the end of the simulation, showing the separation into bounded and free populations.

The connectivity provides an estimate of the escape probability, which increases with the excess of kinetic energy over the field contribution, and with the electric field. The similarity of this scenario to the classical Dreicer threshold is emphasized by the introduction of a 'collisionless Dreicer field'. Whereas in a collisional plasma runaway sets on for the electrons before the ions, this is not so in the collisionless case where the ions become demagnetized before the electrons. The arguments leading to equation (21) are easily generalized to other tilted potentials of the form $\Phi = \Phi(G(\boldsymbol{r}); z)$, which arise, for example, in the quantum Hall effect (Trugman and Weinrib 1983).

It was stated (e.g. Sapoval *et al* 1985) that some aspects of the critical phenomena may persist in non-uniform percolation. For the present model this would imply the existence of a critical energy $E_c < E_c^0$ if $\mathcal{E} > 0$. However, such a critical energy does not exist in a strict sense, because $\lim_{L\to\infty} \tau_z(L) \neq 0$ if $\mathcal{E} > 0$. Nevertheless, the escape probability is strongly suppressed if $E^* < \eta^2 - \Delta E^*$ (equation (22)), and goes over to a step function as $\mathcal{E} \to 0$.

Equation (21) refers to the geometrical properties of Φ only ('static' percolation). The dynamical evolution of percolating particles is beyond the scope of this paper, but a brief numerical check of their long-term behaviour is appropriate. It was mentioned in section 3 that one may expect ergodic behaviour and unbounded motion if a particle is in the infinite accessible domain, which is expected to be the case if the 'collisionless Dreicer' criterion (23) is fulfilled. Within the numerical accuracy, this conjecture is supported by trajectory simulations, an example of which is shown in figure 10. The vector potential has correlation length $l = 20$, the linear system size is $N = 512$, and the dimensionless electric field is $\epsilon = 0.12$. About 10^4 test particles ($q/m = 1$) are integrated forward in time. The boundary conditions are double periodic and the electric field always points in the $+z$ direction, so that every cycle in z increases (or decreases) the kinetic energy by $\pm(N/l)\epsilon$. The simulated duration is $5 \times 10^4\, \Omega_{\delta B}^{-1}$, with $\Omega_{\delta B}$ the gyro frequency due to the rms magnetic fluctuations; this duration corresponds to a distance $\sim$1700 l at free propagation. The initial velocities are isotropic with energies E^* uniform in [0, 1]; the initial positions are uniform in $[0, N] \times [0, N]$. The particles are considered free when their final dimensionless kinetic energy E^* exceeds 10, and bounded if below 10. The initial energy and momentum of free (bounded) particles is marked black (grey) (figure 10, left view). For comparison, the 'collisionless Dreicer' criterion (23) is indicated by a solid line. Most particles fulfilling (23) eventually become free, and the initial population

is separated into bounded and accelerated parts (figure 10, right view), as expected from the assumption of ergodicity. The bounded-free transition is somewhat less sharp than expected from equation (22), which is attributed to the small effective system size $N/l = 25$.

Appendix A. Numerical simulations

The numerical experiments deal with site percolation on a square lattice of linear size $N \leqslant 2^{11}$. For the lattice model, the vertices are independent of each other, and occupied with probability p. In the continuous case, a Gaussian random field $G(\boldsymbol{r})$ is constructed on the square lattice using a standard spectral method with random phases and prescribed power spectrum/two-point function (Martinez *et al* 1992). Each vertex $\boldsymbol{r}_i$ is 'occupied' if $G(\boldsymbol{r}_i) \leqslant h$, and 'vacant' if $G(\boldsymbol{r}_i) > h$. The main difference between the lattice and 'continuum' models is the presence of spatial correlations in the latter. For the sake of digital resolution, $\mathcal{G}'$ is simulated rather than $\mathcal{G}$, which is structurally unstable for $\eta \to 0$. The two-point function of $G(\boldsymbol{r})$ is chosen as $\langle G(0)G(\boldsymbol{r})\rangle = \mathrm{e}^{-r^2/2l^2}$, with $l \geqslant 2$. Avoiding discretization effects requires $l \gg 1$; however, this also decreases the effective system size N/l. Numerous runs were performed with varying N, l and N/l, from which it was found that discretization effects play a substantial role if $l \lesssim 4$, where they shift the critical threshold from the theoretical value $h_c = 0$ up to $h_c \sim 0.03$ (for $l = 1$). Due to its spectral construction, $G(\boldsymbol{r})$ has double periodic boundary conditions, which are also applied to the connected clusters in the uniform dimension(s). Periodic boundaries avoid the situation that large clusters are cut off and counted as artificial fragments. The clusters are classified by a slightly modified version of the classical Hoshen–Kopelman algorithm (Hoshen and Kopelman 1976). The connectivity and cluster diameter distributions are determined from a unique sweep through the N^2 lattice points. Each of the parameter sets $(p, \eta, \epsilon, \ldots)$ is simulated for 10^3–10^5 realizations. The test particle trajectories are computed using a leapfrog scheme which enforces exact energy conservation in the absence of an electric field. All code is written in Fortran 95, and a typical run takes a few days on a medium-size work station.

Appendix B. Properties of $\tau_z(n)$ and $\tau\,(\mathbf{0}, \boldsymbol{e}_\mathrm{n})$

This appendix provides some useful inequalities valid in the subcritical phase. We consider percolation on the square lattice with uniform probabilities p. It is known that $\tau(\mathbf{0}, e_n) \to A(p)n^{-1/2}\,\mathrm{e}^{-n/\xi}$ (Campanino *et al* 1991), and that the connection probability between the origin and the boundary of the quadratic box $B(n) = \{\max(|x|, |z|) \leqslant n\}$ is $\mathrm{Prob}(\mathbf{0} \leftrightarrow \partial B(n)) \sim \mathrm{e}^{-n/\xi}$, with the same correlation length ξ as in $\tau(\mathbf{0}, e_n)$ (Grimmet 1999). Assuming $\tau_z(n) \sim \mathrm{e}^{-n/\lambda}$, we will show that $\lambda = \xi$, and that the exponential ansatz is appropriate. According to its definition, $\tau_z(n) \geqslant \tau(\mathbf{0}, e_n)$, implying $\lambda \geqslant \xi$. On the other hand, $\tau_z(n) \leqslant \mathrm{Prob}(\mathbf{0} \leftrightarrow \partial B(n))$ because each path from the origin to the line $z = n$ must pass (or touch) $\partial B(n)$, indicating that $\lambda \leqslant \xi$. The combination of the two inequalities yields $\lambda = \xi$, and the simultaneous satisfaction of upper and lower exponential bounds justifies, *a posteriori*, the exponential ansatz.

References

Adler R J 1981 *The Geometry of Random Fields* (New York: Wiley)
Ambrosiano J, Matthaeus W H, Goldstein M L and Plante D 1988 *J. Geophys. Res.* **93** 14 383
Arzner K and Scholer M 2001 *J. Geophys. Res.* **106** 3827
Arzner K, Scholer M and Treumann R 2002 *J. Geophys. Res.* at press

Campanino M, Chayes J T and Chayes L 1991 *Prob. Theory Relat. Fields* **88** 269
Chayes J T, Chayes L, Fisher D and Spencer T 1986 *Phys. Rev. Lett.* **57** 2999
Dreicer H 1960 *Phys. Rev.* **117** 329
Edenstrasser J W 1980 *J. Plasma Phys.* **24** 299
Fisher M E 1983 *Lecture Notes in Physics* vol 186 ed F J W Hahne (Berlin: Springer)
Fortuin C M, Kasteleyn P W and Ginibre J 1971 *Commun. Math. Phys.* **22** 89
Gefen Y, Aharony A and Alexander S 1983 *Phys. Rev. Lett.* **50** 77
Greco A, Veltri P, Zimbardo G, Taktashvili A L and Zelenyi L M 2000 *Nonlin. Proc. Geophys.* **7** 159
Grimmet G G 1999 *Percolation* 2nd edn (Berlin: Springer)
Harris T E 1960 *Proc. Camb. Phil. Soc.* **56** 13
Hoshen J 1997 *J. Phys. A: Math. Gen.* **30** 8459
Hoshen J and Kopelman R 1976 *Phys. Rev.* B **14** 3438
Isichenko M B 1992 *Rev.: Mod. Phys.* **64** 961
Jones F C, Jokipii J R and Baring M G 1998 *Astrophys. J.* **509** 238
Kesten H 1980 *Commun. Math. Phys.* **74** 41
Littlejohn R G 1981 *Phys. Fluids* **24** 1730
Martinez V J, Portilla M and Saez D 1992 *Proc. Valencia 1991 Summer School* (Berlin: Springer)
Milovanov A V and Zelenyi L M 1995 *Geophys. Monogr. Service* vol 90 (Washington, DC: AGU) p 357
Milovanov A V and Zimbardo G 2000 *Phys. Rev.* E **62** 250
Nakayama T, Yakubo K and Orbach R L 1994 *Rev. Mod. Phys.* **68** 381
Nienhuis B, Riedel E K and Schick M 1980 *J. Phys. A: Math. Gen.* **130** L192
Riedel E K 1981 *Physica* A **106** 110
Roux S, Hansen A and Hinrichsen E 1990 *J. Phys. A: Math. Gen.* **23** L1253
Sapoval B, Rosso M and Gouyet J F 1985 *J. Phys. Lett.* **46** L149
Schlickeiser R 2002 *Cosmic Ray Astrophysics (Astron. & Astroph. Library Series)* (Berlin: Springer)
Sykes M and Essam J 1964 *J. Math. Phys.* **5** 1117
Treumann R 1997 *Geophys. Res. Lett.* **24** 1727
Trugman S A and Weinrib A 1983 *Phys. Rev.* B **27** 7539
Veltri P, Zimbardo G, Taktashvili A L and Zelenyi L M 1998 *J. Geophys. Res.* **103** 14 897
Weinrib A 1982 *Phys. Rev.* B **26** 1352
Ziff R 1992 *Phys. Rev. Lett.* **69** 2670
Ziff R and Sapoval B 1986 *J. Phys. A: Math. Gen.* **19** L1169